NEW TECHNOLOGIES

CMEIAS JFrad: A Digital Computing Tool to Discriminate the Fractal Geometry of Landscape Architectures and Spatial Patterns of Individual Cells in Microbial Biofilms

Zhou Ji · Kyle J. Card · Frank B. Dazzo

Abstract Image analysis of fractal geometry can be used to gain deeper insights into complex ecophysiological patterns and processes occurring within natural microbial biofilm landscapes, including the scale-dependent heterogeneities of their spatial architecture, biomass, and cell-cell interactions, all driven by the colonization behavior of optimal spatial positioning of organisms to maximize their efficiency in utilization of allocated nutrient resources. Here, we introduce CMEIAS JFrad, a new computing technology that analyzes the fractal geometry of complex biofilm architectures in digital landscape images. The software uniquely features a data-mining opportunity based on a comprehensive collection of 11 different mathematical methods to compute fractal dimension that are implemented into a wizard design to maximize ease-of-use for semi-automatic analysis of single images or fully automatic analysis of multiple images in a batch process. As examples of application, quantitative analyses of fractal dimension were used to optimize the important variable settings of brightness threshold and minimum object size in order to discriminate the complex architecture of freshwater microbial biofilms at multiple spatial scales, and also to differentiate the spatial patterns of individual bacterial cells that influence their cooperative interactions, resource use, and apportionment in situ. Version 1.0 of JFrad is implemented into a software package containing the program files, user manual, and tutorial images that will be freely available at http://cme.msu.edu/cmeias/. This improvement in computational image informatics will strengthen microscopy-based approaches to analyze the dynamic landscape ecology of microbial biofilm populations and communities in situ at spatial resolutions that range from single cells to microcolonies.

Keywords Biofilm architecture · CMEIAS · Fractal geometry · Image analysis · Spatial pattern

Introduction

Since Mandelbrot's 1982 first description of fractals in the natural world and their use to analyze the self-similarity of complex coastlines across a range of spatial scales [1], applications of fractal analysis have rapidly infiltrated through many fields of physics and biology, including ecology [2]. This is largely because fractal geometry provides better quantitative tools than Euclidean models to describe complex natural shapes, and allows for the integration of dynamic factors such as spatial and temporal scales that other methods cannot account for [3].

One of the main problems encountered when describing and modeling spatially distributed landscapes is the natural spatial variability of ecologically vital factors such as the physicochemical environment, biomass and productivity, and hydrological characteristics. Since natural variability is not constant, using simple point models are ineffective. Therefore, the ecological analysis of a landscape system at any spatial scale will benefit by applications of fractal geometry analysis to describe, define, and model its scale-dependent heterogeneity in structure, especially when its architecture has high complexity [3, 4]. Nowadays, the fractal landscape is used as the "default" model where real patterns of complex landscape heterogeneity may be compared quantitatively [2].

A prevailing theme within landscape ecology is to use fractal geometry when analyzing the configurations of spatial

Z. Ji
Department of Systems Biology, Columbia University, New York, NY 10032, USA

K. J. Card · F. B. Dazzo (✉)
Department of Microbiology & Molecular Genetics, Michigan State University, East Lansing, MI 48824, USA
e-mail: dazzo@msu.edu

mosaics since they greatly influence the wide range of ecological phenomena that connect population dynamics and the structure of their habitat [3]. Fractal geometry is better suited to describe these various phenomena because landscape shapes are irregular and fragmented; therefore, they have a greater degree of complexity when compared with Euclidean approximations [5]. For instance, at the core of the allometric scaling relationships between body size and metabolic rate in ecophysiology are the local variations in nutrient resource allocation within habitats being colonized. Acquiring enough food is the first key requirement for successful colonization of habitats in all of biology. Various ecological studies suggest that metabolic processes used for growth physiology rely on the hierarchical, fractal-like nature of resource distribution networks, and that organisms have exploited a fourth spatial dimension by evolving hierarchical fractal-like structured spatial distributions designed to maximize nutrient resource allocation and acquisition [4, 6, 7]. Fractal descriptions of this self-similarity metric for communities provide quantitative insights about the spatial distribution of resources in situ and how organisms exploit and compete for those resources [7, 8]. For instance, fractal geometry has been used to quantify differences in the morphology of growing microbial colonies in relation to resource apportionment within their habitat, and changes induced by the addition of new carbon sources and competing microorganisms to establish their colony systems [5]. This fractal partitioning of heterogeneous distributions and allocations of the same resource is an important trade-off constraint that enables the coexistence of multiple species among community participants [7, 9]. Thus, a fractal analysis of landscapes can provide insights that help to explain the ecophysiology of microbial colonization behavior on surfaces, driven by their nutrient resource allocation and optimal positioning to maximize their utilization efficiency of nutrients [10].

Bacterial biofilms exhibit self-similar fractal geometry at multiple spatial scales [6, 11, 12], reflecting the complex morphology of their microcolony coastline borders that typically result from microhabitat fragmentation and heterogeneity in their resource utilization rates. Some image analysis software applications have included fractal analysis that can analyze and map biofilm architectures [13–15]. Among the freely-available, stand-alone image analysis softwares that include fractal dimension (FD) analysis are ImageJ [16], Fractal Dimension Estimator (www.fractal-lab.org/Downloads/FDEstimator.html), and Fractal3 [17] that use the box count method, and FragStats [18] that uses a perimeter-area regression method to compute fractal geometry of landscapes in digital images. Other free programs include Fractalyse designed for urban planning and feature a combination of box count and dilation methods to analyze fractal geometry [19], and FracTop to analyze branched neurons using the fractal mass-radius method [20].

Many mathematical methods to compute fractal dimension have been proposed and used independently in ecological research [21]. Since each metric quantifies a discrete characteristic of the fractal landscape, there is a need for a well-documented and freely-available image analysis system that takes advantage of the wider range of methods (more so than currently available) to measure fractal dimension, and also features a more comprehensive yet easy to use fractal geometry analysis tool optimized to support microbial biofilm research. An early prototype named Biofilm Image Processing (BIP) was designed and developed [22, 23] to take advantage of the data-mining opportunities made possible by the range of different methods available to compute fractal dimension. However, BIP was implemented in an obsolete version of Microsoft Visual Studio and was no longer supported. Later, we recognized the benefits of using multiple methods of fractal dimension analysis (as originally implemented in BIP) to discriminate biofilm architectures. Therefore, we have recreated this opportunity to data-mine the fractal analysis of biofilm architectures by developing an improved reimplementation of BIP software. Here, we introduce this new software application, named CMEIAS JFrad, that uniquely features a comprehensive collection of 11 different fractal dimension methods implemented into a semi-automatic wizard designed to maximize ease-of-use for analysis of biofilms and other landscapes in single images, or multiple images in an automated batch process. We also describe the protocols of CMEIAS JFrad to rank the importance of different fractal analysis methods that discriminate biofilm architecture, to optimize the variable settings of key image processing steps that must precede fractal analysis, and examples of its use to compare the spatial ecology of microbial biofilm landscapes.

Materials and Methods

Coding Information

CMEIAS JFrad code is implemented using Java and so all features are easily available to both Windows and non-Windows users. Java 6 or higher (freely available at https://www.java.com/en/) must be installed in order to run JFrad.

Biofilm Development, Microscopy, and Image pre-Processing

Clean borosilicate glass microscope slides (considered "control") and polylysine-coated glass slides were submerged for four summer days from a fishing line approximately 1 ft below the surface of the Red Cedar River that flows through the campus of Michigan State University (East Lansing, MI, USA). Slides were retrieved, their underside wiped clean,

mounted in filter-sterilized water with a No. 1.5 thickness glass cover slip, and examined by brightfield light microscopy using a 1× and 10× Neofluor objective lens. Digital 8-bit grayscale images of the freshwater microbial biofilms developed on control glass and polylysine-coated glass were acquired using a monochrome digital camera, processed to invert their image brightness table (dark→light, light→dark) using Adobe Photoshop CS3, and analyzed using CMEIAS JFrad.

Data Analysis

The output data of biofilm fractal dimensions were saved as *csv files and analyzed statistically using the StatistiXL addin [24] running within Microsoft Excel.

Results and Discussion

Software Logic of Mathematical Methods Used by JFrad to Analyze Fractal Dimension

The term "fractal dimension" can be used in a more general sense referring to any of the dimensions commonly used to characterize fractals [25]. Most commonly it is used in its narrowest meaning, i.e., capacity dimension [26] according to the following:

$$d_{\text{capacity}} \equiv - \lim_{\epsilon \to 0^+} \frac{\ln N}{\ln \epsilon} \qquad (1)$$

where N is the number of elements forming the finite cover and ε is the size of each element. For a straight line, this value is evaluated to be 1 because $N=1/\varepsilon$; for a 2-dimensional shape, say, a square, the value is 2 because $N=1/\varepsilon^2$; for a fractal, d_{capacity} is typically a value between 1 and 2, indicating its departure from Euclidian geometry.

The fractals of interest in the image are not the objects themselves (e.g., biofilm microcolonies), but rather the complexity of their border coastlines. Furthermore, such "fractals" in a digital image are not fractal in the strictest sense of being self-similar over all spatial scales because of the finite size of the pixels [27, 28]. In a digital image, the pixel is the smallest scale that can be evaluated and the mathematical limit is interpreted as over the extrapolation. However, if the image represents some real objects that are fractals, the fractal dimension of the object (or its borders) can be evaluated using the shapes defined by the pixel values. The relationship between such evaluation and the real fractal dimension is mathematical and is based on the assumption that the underlying objects, or more precisely their border coastlines, are really fractals.

CMEIAS JFrad typically analyzes digital binary images in which the pixels of the foreground objects (e.g., individual cells or microcolony biofilms) are represented by pure white color against a black background. The program utilizes a user-defined brightness threshold setting to convert the input image if not already binary (methods to optimize that setting are described here). Eleven mathematical methods are implemented to evaluate the fractal dimension of the 2-dimensional border coastline of those foreground objects, not their volume, mass, or surface texture (lacunarity). These eleven fractal methods can be categorized into four groups. Group 1 is based on the purely pixel-represented borders, i.e., individual objects are not differentiated. Group 2 is based on the so-called "traced-border", i.e., each object is considered separately and the sequential order of its border pixels is used in the procedure of evaluation. Group 3 is based on mass-based methods. Although the mass here actually refers to the mass of the border, this group of methods treats the border (represented either as simply a set of pixels or a traced pixel sequence) as a solid object instead of merely a digital representation of the width-less separation between the real object and its immediate surroundings. Group 4 is based on the concept of "corners" along the border. All the methods follow the same pattern: for a sequence of an incremental variable , the method-specific image measurement A is calculated for each value of r; then a linear regression is used to obtain the slope of the log−log plot of A vs. r; and finally the fractal dimension is then evaluated by some simple conversion from the slope.

We will use the term "the slope of the $\log(A) \sim \log(r)$" in the following description. The slope with the simple notation of:

$$\text{slope} \sim \frac{y}{x}$$

is defined, for a sequence of y: $y_1, y_2, \cdots, y_n$ and a sequence of x: $x_1, x_2, \cdots, x_n$, as the regression coefficient b for the linear least squares fitting [29] of y_i versus x_i in: $\hat{y}_i = a + bx_i$. We will denote the fractal dimension as D_f.

Group 1 Methods Based on Simple Length-Related Pixel Borders

The first method in Group 1 is called "dilation" [30–32]. It represents the dilation of the borders and has the following algorithm-specific features: let r be the radius of dilation, A be the area of the dilated border, slope~$\log A/\log r$, $D_f=2-$slope, and $d=2r$ (called the "kernel diameter"). For a straight line, A/d is constant so the slope is 0 and $d=1$. When log (A/d) vs. log (d) is linear, then A/d vs. d is exponential, so A vs. d is exponential as well.

The second method in Group 1 is called the "Euclidean Distance Map." It has the following algorithm-specific features: let d be the shortest Euclidean distance to the border pixels, A be the area within that distance, slope~$\log A/\log d$

and $D_f = 2 -$ slope. The direct difference between this method and the dilation method described above is that the Euclidian distance used here is based on the original border pixels. In the dilation method, the new area at each step is based on the previous step, not the original starting status.

The third method in Group 1 is called "box counting" (also known as the "grid" method [33]. It has the following algorithm-specific features: let a be the box size (i.e., the number of pixels on each side of the square area), N be the number of boxes covering all border pixels,in terms of the number of pixels; slope~$\log N/\log a$, and $D_f = -$ slope.

Group 2 Methods Based on Traced Borders [34–36]

The three methods in this group treat the border of each individual object as a sequence of pixels.

The first method in Group 2 is called "fast." It has the following algorithm-specific features: let a be the interval between pixels, in terms of the number of pixels; L be the perimeter connecting the interval pixels, slope~$\log L/\log a$ and $D_f = 1 -$ slope.

The second method in Group 2 is called "fast (hybrid)." It has the following algorithm-specific features: let a be the distance interval between pixels along the traced border, L be the perimeter connecting the interval pixels, slope~$\log L/\log a$ and $D_f = 1 -$ slope. This method is similar to the fast method except that each pixel connects to the closest pixel at least distance a away. By contrast, in the fast method, the pixel connects to the next pixel by skipping $a - 1$ pixels between them.

The third method in Group 2 is called "parallel lines." It has the following algorithm-specific features: let d be the interval between parallel horizontal lines, L be the perimeter connecting the pixels on those lines along the traced border, slope~$\log L/\log d$, and $D_f = 1 -$ slope. This method is also similar to the fast and fast (hybrid) methods, but with it each segment along the perimeter is more likely to be different. Conceptually, the parallel lines could be chosen as vertical instead of horizontal lines, and the choice is arbitrary.

Group 3 Methods Centered on Mass-Based Borders [31]

Like in Group 2, methods in Group 3 are based on the pixel boundary but treat it differently as mass instead of boundary.

The first method in Group 3 is called "cumulative intersection." It has the following algorithm-specific features: let r be the radius of the circle, A be the area of the object within the circle, slope~$\log A/\log r$, and $D_f =$ slope. The area is decided as the count of the pixels within the circle. This method was originally used to describe the fractal dimension of neurons [33] or the cross-section of some objects, meaning it has a core and the algorithm starts reasonably from radius 0 or a very small radius. In the case of the "blob-like" microcolonies commonly occurring in microbial biofilms, the cumulative

intersection method regards the border pixels instead of the original blobs as the "objects." Otherwise, the resulted fractal dimension will always be a number very close to 2, not what we really want to evaluate in this case.

The computation of the fractal dimension using the cumulative intersection method could return a result outside the range of 1.0–2.0, which is only a numeric artifact. When the growing circle of enclosure exceeds the size of the object, then the cumulative intersection will not increase, the slope and the calculated fractal dimension will decrease below 1 and could even approach 0. Consequently, the cumulative intersection method is designed to stop once the circle of enclosure grows beyond the entire object. On the other hand, if there is a hole inside the "object," the increment of cumulative intersection count will be faster than the entirely filled area and result in a calculated fractal dimension that is larger than 2. There are two possible ways to avoid this illogic result: either add one pixel for a given circle that contains no pixel, or start the method only when it actually intersects the objects. There are two shortcomings for the second situation that must be accommodated. First, the fractal dimension can still be larger than 2.0 if it requires only a few steps that produce a very large slope. For example, a pixel count of 1, 10, 1000, and 1,000,000,000 is theoretically possible when not starting from the origin (usually the object's center). Second, in the case of multiple separated objects in the image, the existing space between them will cause JFrad to calculate a fractal dimension that is either much larger or smaller than the actual object's fractal dimension in a misleading way. So, the final algorithm implemented into JFrad to handle these scenarios is thus designed so that each object is handled separately, i.e., each object's iteration starts from the original and one artificial pixel is added if there is an internal hole; then, the ultimate result is an accurate average of the fractal dimensions of all objects weighed on each object's pixel's count.

The second method in Group 3 is called "mass radius (long)." It has the following algorithm-specific features: let r be the radius of the circle around chosen border pixels, A be the area of the objects (total pixel count) within the circles, slope~$\log A/\log r$, and $D_f =$ slope. Conceptually, this method does not need traced borders. However, using both the pixel array and the traced list of the borders, the algorithm can be implemented more efficiently.

The third method in Group 3 is called "mass radius (short)." It has the following algorithm-specific features: let r be the radius of the circle around chosen border pixels, A be the area of objects (total pixel count) within the circles, slope$= \log A/\log r$, and $D_f =$ slope. This method uses the same strategy as the mass radius (long) except that only a subset of pixels are used as the object centers to evaluate mass radius, whereas the mass radius (long) version uses all the object pixels. The

subset can be chosen randomly [22]. This method generally needs to use traced borders.

Group 4 Methods Based on Corner-Analysis

The two methods in this group are based on the traced borders of the objects within the image [22]. They are sensitive to the selection of the control parameters and are more likely than other methods to produce numeric results that are out of the theoretical range of 1–2. A corner is defined as the pixel along the object's border, or vertex, whose height is at least h. The concept of the height is defined for vertex P_i as the distance from the vertex P_i to the line P_0P_{i+1}, where P_0 is a reference point and P_{i+1} is the following pixel along the traced border. After a corner is found, it serves as the reference point to search for the next corner along the traced border of the objects.

The first method in Group 4 is called "corner count." It has the following algorithm-specific features: let h be the minimum height to define a corner, N be the number of the corners, slope~$\log N/\log h$, and $D_f=-$slope.

This method is based on the assumption that on a fractal, the largest size of "corners" being considered, as represented by S, is related to the number of such corners, n, in this way:

$$O\left(\frac{1}{S}\right) \leq n \leq O\left(\frac{1}{S^2}\right) \tag{3}$$

This translates to $-2 \leq \log n/\log S \leq -1$. So, the fractal dimension is evaluated as $-$slope, which will be between 1.0 and 2.0. The actually pixel-represented objects may not satisfy the

above assumption though. Consequently, it is still possible to get a result outside of the range between 1.0 and 2.0. This relationship is meaningful when considering the limit of $S \rightarrow 0^+$ but definitely not when $S \rightarrow \infty$. So, the larger S should be considered less desirable than the smaller S. Much of the discussion of this method also applies to the corner (perimeter) method described next.

The second method in Group 4 is called "corner perimeter." It has the following algorithm-specific features: let h be the minimum height to define a corner, L be the perimeter connecting all the corners, slope~$\log L/\log h$, and $D_f=1-$slope. This method is based on the assumption that on a fractal object, the largest size of its "corners" being considered, represented as S, is related to the perimeter connecting such corners, p, in this way:

$$O(1) \leq p \leq O\left(\frac{1}{S}\right) \tag{4}$$

This translates to $-1 \leq \log p/\log S \leq 0$. So, the fractal dimension is evaluated as $1-$slope, which will lie within the range between 1 and 2.

Fractal Analysis Protocol Using CMEIAS JFrad

JFrad supports multiple image formats, including tiff, bmp, png, jpg, and gif. Input images can be either 8-bit grayscale or 24-bit RGB images. Its graphical user interface (Fig. 1) has a semi-automated wizard design to maximize ease-of-use for analysis of biofilms and other landscapes in single images and a fully automated mode for analysis of multiple images in a

Fig. 1 CMEIAS JFrad graphical user interface and fractal analysis of a single biofilm image. Shown is the input biofilm image [21] (a open image), and the output images produced at each intermediate step of the wizard sequence for fractal analysis, b binarize, c remove small particles, d fill holes, e decide border, and f calculate fractal dimension. The *right panel* (*F*) displays the basic image statistics and fractal dimension data after completion of the final step. The specifications of control parameters to perform these steps are entered in the Option>Setting menu
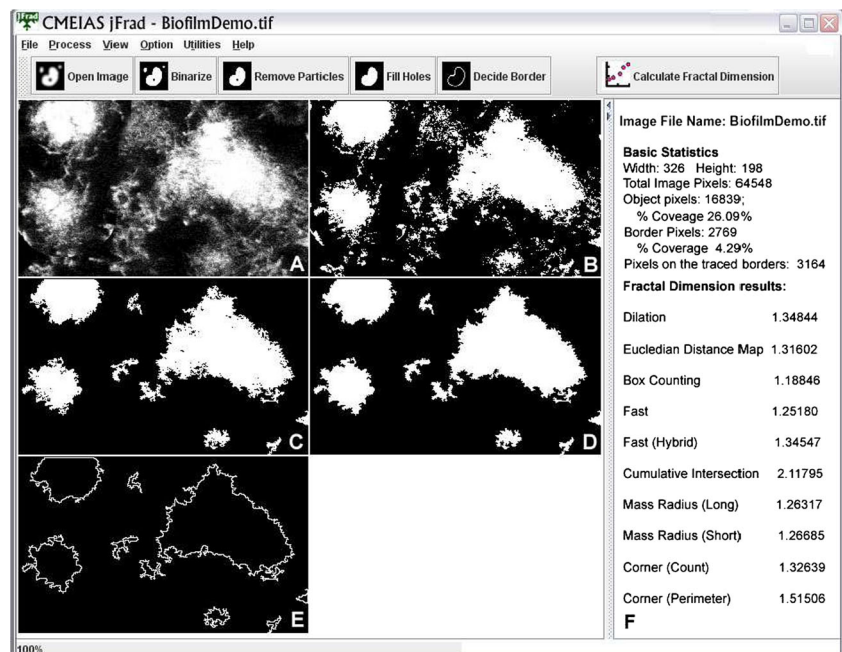
batch process. Before starting the image processing and analysis sequences, the user should specify several control parameters (Main Menu Option>Settings), including the percentage or brightness method and its threshold boundary used to find and binarize the objects, the maximum particle size (pixels) to be removed as background, the maximum internal hole size (pixels) to be filled, the selection of any combination of the eleven methods of fractal dimension for analysis, and the decimal precision to display the fractal dimension output (default is 5). The wizard sequence to analyze a single image (Fig. 1a–f) is open image→binarize→remove particles→fill holes→decide border→calculate fractal dimension→copy/print/save data output. At any step of this sequence, the current processed image in the GUI can be copied to the clipboard and saved (default in bmp format). The data output for analysis of individual images (Fig. 1f) includes the file name of the input image, its pixel dimensions (width/height/total area), the cumulative number of pixels of all foreground objects and their traced borders, the % of the input image pixels covered by the area and border of all foreground objects, and the fractal dimensions of the foreground objects in the landscape image calculated by each of the user-selected methods. To analyze multiple images in a batch process, the user first builds a suitable batch folder containing the images of interest, then indicates its location (Main Menu File>Open Image Directory), and finally specifies the name and location of the output data file (automatically saved in *.csv format) containing a table that lists rows of the individual image names and their fractal dimensions calculated by each of the user-selected methods. A progression bar displays when the automated batch analysis commences, informing the user about its present status and final completion.

Optimizing the Default Settings of Minimum Object Size and Brightness Threshold

The default settings of some control parameters in JFrad (Option>Settings) are arbitrary, including the choices of maximum hole size to be filled within foreground objects, methods to threshold and find object borders, iteration parameters, and decimal precision of the reported fractal dimension value. The challenge to explore their effects on the estimated fractal dimension of biofilms is simplified by using its wizard design. Aside from these, the minimum object size and brightness threshold values represent two important settings that can significantly influence the amount of fractal dimension detected in digital images of immature microbial biofilms acquired at spatial scales that resolve microcolonies. Both variables should be optimized experimentally since they greatly influence the signal-to-noise relationship of image segmentation that classifies the pixels as either foreground objects of microcolony biofilms to be retained and analyzed, or as background to be excluded from analysis. The goal is to use optimal settings of these two parameters that will exclude the microcolony "noise" or invalid objects that are smaller than the specified minimum size and/or darker than the minimum brightness threshold. The noise of very small microcolonies in the biofilm landscape images may be abundant, lack fractal geometry, and/or can overwhelm the discriminatory analysis of larger microcolonies in immature biofilms. Examples of applying the brightness threshold and minimum object size processes to a landscape biofilm image are illustrated in Fig. 1b, c. The following section describes how these two settings were optimized and implemented as default in JFrad. A similar examination is recommended when investigating other biofilms.

We used the automated batch process mode of JFrad to analyze 50 inverted-brightness images of the freshwater biofilm communities, 25 of which sample the biofilm developed on control glass slides and 25 on polylysine-coated glass slides. These two biofilm landscapes differ in microcolony architecture because of their different colonization behaviors on physicochemically dissimilar substrata (Fig. 2a, b).

The first set of experiments was designed to identify the optimal decision boundary of minimum object size for measurement of fractal dimensions in these two biofilm landscapes. The fractal dimension of each image was analyzed using all 11 methods, with the minimum object size set at ten different pixel values while maintaining the brightness threshold at a constant setting of 125 gray level and the maximum

Fig. 2 Representative brightness inverted micrographs of freshwater biofilm communities developed for 4 days on microscope slides of **a** control glass and **b** polylysine-coated glass and acquired using the 10× objective lens. *Bar scales* are 100 μm
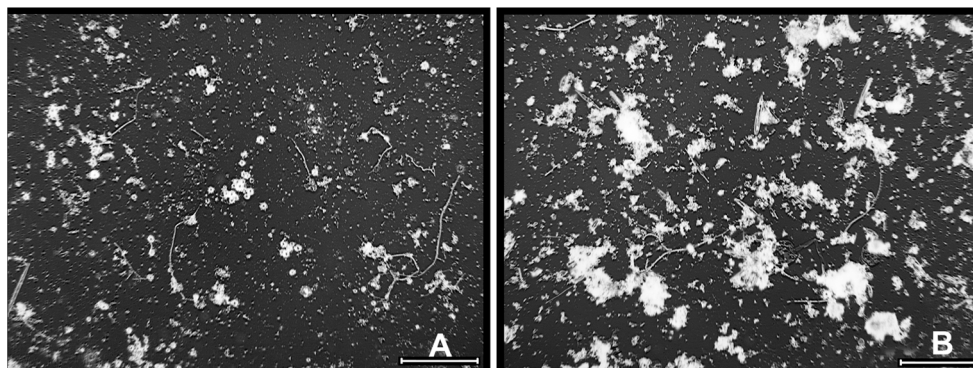
Table 1 Univariate analysis of variance of the minimum object size for freshwater aquatic biofilms developed on plain glass slides or polylysine-coated glass slides and measured by 11 mathematical methods of fractal dimension[a]

Fractal dimension method	Control glass	Polylysine substratum
Corner (perimeter)	4.428	5.664
Box counting	11.027	0.786
Mass radius (long)	41.951	9.496
Dilation	42.204	7.368
Mass radius (short)	43.479	9.580
Euclidean distance map	55.840	11.614
Cumulative intersection	58.123	74.654
Corner (count)	92.472	53.513
Parallel lines	178.849	130.969
Fast (hybrid)	378.259	240.329
Fast	412.763	228.216

[a] Reported values are the Anova F statistic, and all were highly significant at $p < 0.000$ except for the polylysine biofilm measured by the box counting method ($p = 0.629$)

hole size to be filled at 300 pixels. A univariate analysis of variance [24] indicated that the fractal dimension methods differ significantly in their ability to detect fractal geometry in these biofilms, and a ranked order evaluation indicated that the fast method was most influenced by variations in minimum foreground object size for the biofilm on the control glass slides and the fast (hybrid) method for the biofilm on the polylysine-coated slides (Table 1). The post hoc Tukey Q multivariate test [24] was then performed to measure the significance in mean differences between nine pairs of minimum object sizes (5 pixel reference vs. 10, 15, 20, 25, 50, 75, 100, 125, and 150 pixels) using these optimized fractal dimension methods. Plots of the sum of post hoc Tukey Q values that were statistically significant (p ranged from <0.000 to 0.049) for each pair of minimum object sizes were similar for both biofilm types (Fig. 3).

To finalize the decision of the default setting value for minimum object size, we further evaluated the differences in Tukey Q values between closest pairs [24]. Using the highest discriminating fast method for the biofilm developed on control glass slides, the difference in Q values between the 50 and 75 pixel sizes was statistically significant ($p = 0.002$), but was not statistically different between the 75 and 100, the 100 and 125, and the 125 and 150 pixel sizes ($p = 0.335$, 0.934, and 0.994, respectively). Using the fast (hybrid) method applied to images of the biofilm developed on polylysine-coated glass slides, the difference in Q values between the 50 and 75 pixel sizes was statistically significant ($p = 0.004$), but was not statistically different between the 75 and 100, the 100 and 125, and the 125 and 150 pixel sizes ($p = 0.669$, 0.994, and 1.000, respectively). Based on these similar statistical results obtained with both biofilm types, we assigned the optimal minimum object size of 75 pixels as default for JFrad.

The second set of experiments followed a similar protocol to identify the optimal setting for the brightness threshold value of the gray level (on a scale of 0 for pure black to 255 for pure white) used by JFrad to classify pixels in the inverted image as either foreground objects (≥threshold) or excluded as background (<threshold). With settings of 75 pixels for minimum object size and 300 pixels for maximum hole to be filled, we measured the fractal dimension of the aquatic biofilms developed on control glass slides and polylysine-coated slides over a range of ten different grayscale brightness values (5, 10, 15, 20, 25, 50, 75, 100, 125, and 150). The univariate analysis of variance [24] indicated that the cumulative intersection method was most sensitive to variations in brightness threshold settings among the 11 fractal dimension methods for both biofilm types (Table 2).

The post hoc Tukey Q test [24] was then performed to measure the difference in means of fractal dimension between nine pairs of the brightness threshold values (reference value of 5 vs. 10, 15, 20, 25, 50, 75, 100, 125, and 150 brightness) using the optimized cumulative intersection method. The sum of statistically significant Tukey Q values (p range from
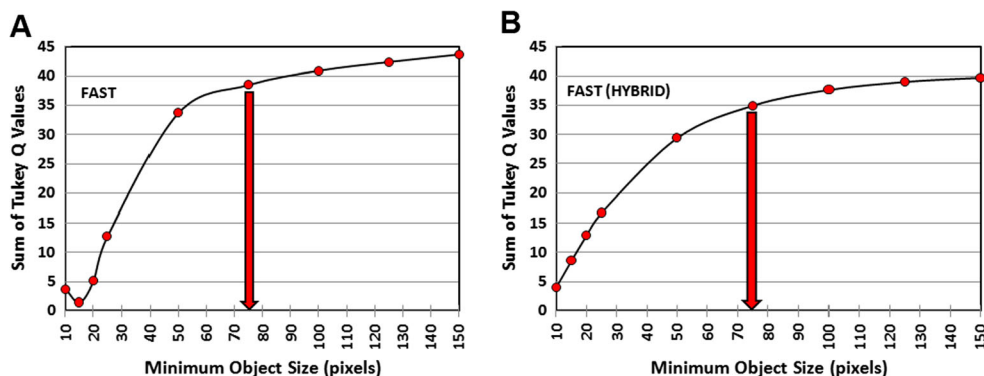

Fig. 3 Optimization of the minimal object size setting for the fractal analysis of the aquatic biofilm developing on control glass slides (**a**) and polylysine-coated glass slides (**b**) using the optimized fast and fast (hybrid) methods of fractal dimension analysis, respectively. All plotted values that were significantly different ($p < 0.05$) from the 5 pixel reference value are noted with an *asterisk*. The *down arrow* denotes the 75 pixel minimum object size assigned as default for JFrad

Table 2 Univariate analysis of variance of the brightness threshold value for fractal analysis of the biofilms developed on control glass slides and polylysine-coated slides measured by 11 mathematical methods of fractal dimension[a]

Fractal dimension method	Control glass substratum	Polylysine substratum
Corner (perimeter)	2.492	2.896
Box counting	35.354	106.281
Euclidean distance map	38.347	97.215
Dilation	51.618	130.940
Mass radius (short)	57.016	103.586
Mass radius (long)	58.743	109.012
Corner (count)	59.468	60.195
Fast (hybrid)	128.854	217.430
Fast	166.970	281.725
Parallel lines	175.567	277.601
Cumulative intersection	319.005	445.631

[a] Reported values are the Anova F statistic, and all were highly significant at $p < 0.000$ except for the control glass and polylysine biofilms measured by the corner (Perimeter) method ($p = 0.010$ and $p = 0.003$, respectively)

< 0.000 to 0.049) for each pair of brightness threshold settings for the biofilms developing on control glass slides and polylysine-coated slides are presented in Figure 4. The results for both biofilms indicated an ascending slope of influence of the brightness threshold setting with an apparent asymptote value of 50. Validation of this value to assign as the default was done by a similar statistical method as described above for minimum object size. Using the cumulative intersection method applied to images of both biofilm types, the difference in Tukey Q values between incremental pairs of 50 and 75, 75 and 100, 100 and 125, and 125 and 150 brightness were not statistically significant ($p = 0.973$, 0.989, and 0.899, and 0.934, respectively, for the biofilm on control glass, and $p =$

1.000 for all pairs for the biofilm on polylysine-coated slides). This statistical result confirmed the choice of 50 as the optimal default brightness threshold setting for JFrad analysis of these biofilm images.

Data-Mining Analysis of Biofilm Architecture by Fractal Geometry

The unique design of JFrad to include 11 different methods to measure the fractal geometry of digital landscapes in the fully automated batch mode facilitates the analysis, especially when the most discriminating FD methods are not known in advance. This analysis of unobvious patterns that transform into useful data creates a "data-mining" opportunity, thereby significantly increasing the probability of finding the best fractal dimension method(s) to discriminate landscapes that may not be apparent if using software featuring only one or a few methods for comparison. As an example of application, we measured the fractal coastline complexity of biofilm landscapes containing microcolonies developed on control glass slides and polylysine-coated slides at two spatial scales (acquired using 1× and 10× microscope objective lenses, and optimal control parameter settings). The results (Table 3) indicate that both biofilms exhibit fractal geometry at multiple spatial scales, and the ability of this characteristic to discriminate their architecture is significantly influence by the FD method(s) used.

Analysis of variance [24] indicated statistically significant differences in fractal geometry between the two biofilm types using four of the eleven FD methods (mass radius-short, mass radius-long, Euclidian distance map, and dilation) when examined at the 1× spatial scale, and using five other FD methods (box counting, fast, fast hybrid, corner count, and parallel lines) when examined at the 10× spatial scale (Table 3). The differences in fractal geometry between the two biofilm types were significantly greater (lower p values)

Fig. 4 Optimization of the brightness threshold setting for the fractal dimension analysis of the aquatic freshwater biofilms developing on control glass slides (*closed circle*, *solid line*) and polylysine-coated glass slides (*triangle*, *dash line*) using the optimized cumulative intersection method. *Plotted values with an asterisk are significantly different from the 5 brightness reference value*. The *down arrow* denotes the 50 grayscale brightness threshold assigned as default for JFrad
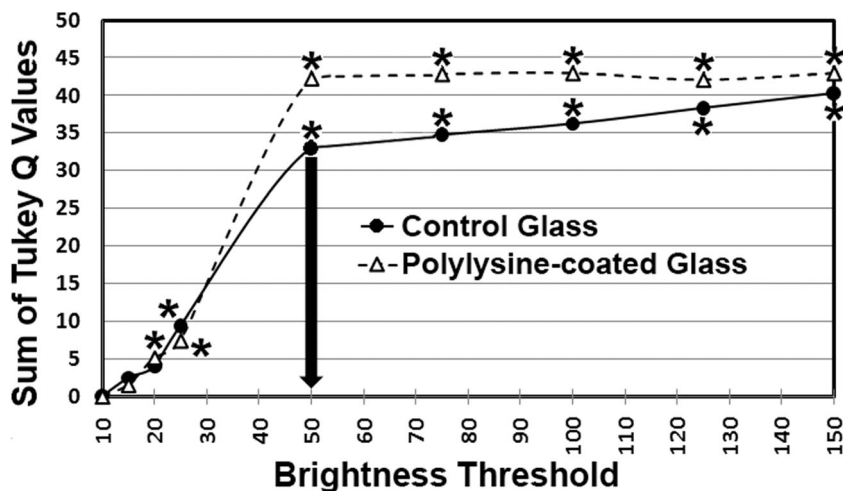
Table 3 Fractal analysis of freshwater biofilms developed on control glass slides and polylysine-coated slides at 2 spatial scales. Images were acquired using 1× and 10× microscope objective lenses

Fractal dimension method	1× Spatial scale				10× Spatial scale			
	Mean control glass	Mean polylysine	Anova F	Prob.	Mean control glass	Mean polylysine	Anova F	Prob.
Corner (perimeter)	1.55471	1.56489	0.128	0.724	1.60254	1.60217	0.00123	0.972
Mass radius (short)	1.41980	1.37548	13.189[a]	0.002	1.31903	1.32135	0.03401	0.854
Mass radius (long)	1.41787	1.37497	12.175[a]	0.003	1.31799	1.32073	0.04791	0.828
Euclidean distance map	1.50314	1.45163	6.171[a]	0.023	1.36137	1.37822	1.31689	0.257
Dilation	1.54301	1.49521	4.967[a]	0.039	1.40010	1.41879	1.63548	0.207
Cumulative intersection	1.74182	1.82268	1.584	0.224	1.83456	1.86489	2.37202	0.130
Box counting	1.59186	1.53823	1.912	0.184	1.35243	1.41140	5.56434[a]	0.022
Fast	1.24565	1.23968	2.302	0.147	1.24358	1.22931	19.81396[a]	5×10^{-5}
Fast (hybrid)	1.28094	1.27644	1.126	0.303	1.29313	1.27036	39.06367[a]	1×10^{-7}
Corner (count)	1.45710	1.44266	0.294	0.594	1.38296	1.45969	68.72056[a]	8×10^{-11}
Parallel lines	1.33275	1.34004	1.208	0.286	1.36635	1.32785	80.63050[a]	8×10^{-12}

[a] Statistically significant differences ($p<0.05$) between the fractal dimensions of the biofilms developed on slides of control glass vs. polylysine-coated glass measured by the same method

using images acquired at the 10× spatial scale than at the 1× spatial scale. These results indicate that both biofilm architectures have fractal geometry at multiple spatial scales, the comprehensive collection of fractal dimension methods featured in JFrad provides sufficient versatility to detect significant differences between biofilms, and the methods with greatest discriminating power are not necessarily the same when biofilms are analyzed at all spatial scales.

Distinguishing Spatial Patterns of Single Cells in Biofilms by Fractal Analysis

Quantifying the spatial heterogeneity of microbial biomass in situ can reveal important insights into their colonization behavior in spatially structured landscapes, such as what typically occurs during biofilm development [10, 37, 38]. Spatial analyses that find patterns of distribution with significant departure from complete spatial randomness indicate that operations of colonization behavior involve a spatially explicit process with unique causes and biological consequences rather than occurring randomly and independent of their location [10, 11]. Also, fractal dimension analysis can provide insights into various ecophysiological activities of colonization behavior that relate to the fractal-like apportionment and use of limiting nutrient resources [7, 10]. For instance, spatial patterns with fractal geometry result from optimal cellular positioning of organisms to maximize their utilization efficiency of allocated nutrient resources during colonization of a landscape, and how the fractal nature of food cluster availability and local concentration enable the coexistence of multiple species among community members [5, 7]. Thus, fractal dimension analysis can be a useful measure of the space-time

complexity of surface colonization and provides several advantages over other descriptive indices of ecological patchiness [5].

We prepared and examined a set of test images containing 1, 2, and 3 identical repeats of 14 microbial cells arranged in clustered, random, and uniform spatial patterns (Fig. 5a–c) to determine if fractal dimension analysis can discriminate these different types of biofilm colonization behavior. Statistical analysis of the results indicated that three of the fractal dimension methods featured in JFrad (dilation, Euclidian distance
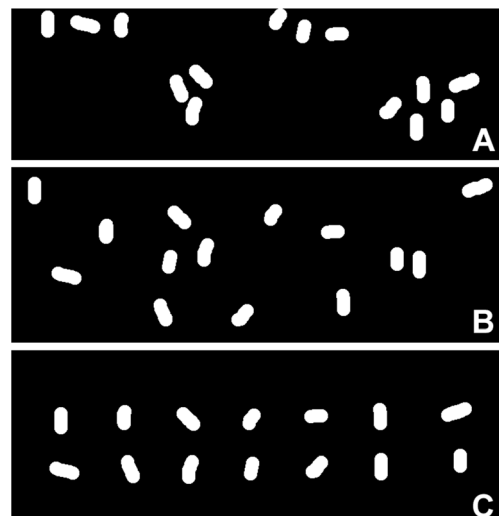

Fig. 5 1× version of 3 distinct spatial patterns of the same 14 identical cells arranged in a study area. The patterns of spatial distribution are clustered (**a**), random (**b**), and uniform (**c**). These three images were the sources to make the 2× and 3× versions of the same individual cells that were included to determine which fractal dimension method(s) can discriminate these spatial patterns independent of object shape and sample size

Table 4 Discrimination of the spatial patterns of distribution among bacterial cells by fractal dimension analysis[a]

Fractal dimension method	Anova F (p value)	Spatial pattern	Mean +/− std. dev.	Pattern pair difference (Tukey Q; p values)
Euclidean distance map	3413.03 (6.77×10^{-10})	Clustered	1.17429 ± 0.00055	C>U $(110.436; 4.93 \times 10^{-8})$
		Random	1.14758 ± 0.00072	C>R $(88.263; 4.92 \times 10^{-8})$
		Uniform	1.14087 ± 0.00002	R>U $(22.173; 1.04 \times 10^{-5})$
Dilation	1565.77 (6.99×10^{-9})	Clustered	1.22470 ± 0.00082	C>U $(75.928; 4.86 \times 10^{-8})$
		Random	1.19159 ± 0.00147	C>R $(58.743; 3.73 \times 10^{-8})$
		Uniform	1.18225 ± 0.00017	R>U $(16.556; 5.77 \times 10^{-5})$
Box counting	132.43 (1.09×10^{-5})	Clustered	1.17466 ± 0.00784	C>U $(21.982; 1.10 \times 10^{-5})$
		Random	1.09632 ± 0.00872	C>R $(16.898; 5.13 \times 10^{-5})$
		Uniform	1.07274 ± 0.00748	R>U $(5.084; 2.66 \times 10^{-2})$

[a] Reported values are the statistical analyses of the fractal dimension of the 1× (14 cells), 2× (28 cells), and 3× (42 cells) images derived from the 1× (14 cells) images in Fig. 5a–c analyzed by the indicated fractal dimension methods. Only these three fractal dimension methods featured in JFrad provided statistically significant discrimination of all three spatial patterns at all three tested abundances

map, and box counting) had significant discriminating power to distinguish these three patterns of spatial distribution from each other at the 1×, 2×, and 3× abundance levels (Table 4), further illustrating the data-mining benefit of including a comprehensive collection of methods for analysis of biofilm architecture. All three of the Group 1 methods indicated that the means of the fractal dimension values have a statistically significant ranked order of clustered>random>uniform. This ranking of the spatial patterns is indicative of the scale-dependent heterogeneous fractal variability in limiting resource partitioning, and reflects the high efficiency at which cells actively disperse and cooperatively position themselves spatially and physiologically when faced with the interactive forces of microbial coexistence to optimize their allocation of nutrient resources on a local competitive scale [5–7, 10, 27, 37, 38]. Thus, fractal discrimination of aggregated vs. random vs. uniform (overdispersed) distribution patterns provides a significant insight into the microbial colonization behaviors that direct biofilm development, where these competitive or cooperative forces are dependent in part on limiting nutrient partitioning and allocation [7, 10, 37, 38].

Concluding Statements

Concepts derived from fractal theory are fundamental to an understanding of the landscape complexity of scale-related phenomena in ecology [3–7]. Fractal geometry can be used to gain deeper insights into complex ecological patterns and processes occurring within natural landscapes, including the scale-dependent heterogeneities of spatial architecture, biomass and ecophysiology of colonization behavior, all driven by the ecological theory of optimal spatial positioning of organisms to maximize their efficiency in utilization of allocated nutrient resources [5–7, 10]. Here, we introduced CMEIAS JFrad, a new computing technology of image processing and analysis for research and educational applications to analyze the fractal geometry of foreground objects in digital images of complex landscapes. JFrad uniquely features a data-mining opportunity based on a comprehensive collection of 11 different fractal dimension methods implemented into a wizard design to maximize ease-of-use for semi-automatic analysis of single images or fully automatic analysis of multiple images in a batch process. As examples of application, quantitative analyses of fractal dimension are used to discriminate the complex architecture of freshwater microbial biofilms at multiple spatial scales and the positioning of individual cells to optimize their spatial patterns indicative of cooperative interactions, resource use, and apportionment in situ. Version 1.0 of JFrad will be implemented into a software package containing the program files, user manual, and tutorial images, and provided as a freely available download at http://cme.msu.edu/cmeias/. This improvement in computational image informatics adds to our CMEIAS suite of integrated software whose combined mission is to strengthen microscopy-based

approaches for advancing a greater understanding of microbial ecology in situ at spatial resolutions that range from single cells to microcolonies.

References

1. Mandelbrot BB (1982) The fractal geometry of nature. W. H. Freeman and Co, New York
2. Halley JM, Hartley S, Kallimanis AS, Kunin WE, Lennon JJ, Sgardelis SP (2004) Uses and abuses of fractal methodology in ecology. Ecol Lett 7:254–271
3. Ruis J (2014) http://www.fractal.org/Bewustzijns-Besturings-Model/Application-Fractal-Geometry.pdf, The Application of Fractal Geometry to Ecology. (2014) Accessed 6 May 2014
4. Sugihara G, May RM (1990) Applications of fractals in ecology. TREE 5:79–86
5. Seuront L (2010) Fractals and multifractals in ecology and aquatic science. CRC Press, Taylor & Francis Group, Boca Raton
6. West G, Brown J, Enquist B (1999) The fourth dimension of life: fractal geometry and allometric scaling of organisms. Science 284:1677–1679
7. Ritchie ME (2010) Scale, heterogeneity, and the structure and diversity of ecological communities. Princeton University Press, Princeton
8. Milne BT (1992) Spatial aggregation and neutral models in fractal landscapes. Amer Nat 139:32–57
9. Palmer M (1992) The coexistence of species in fractal landscapes. Amer Nat 139:375–397
10. Dazzo FB, Klemmer KJ, Chandler R, Yanni YG (2013) *In situ* ecophysiology of microbial biofilm communities analyzed by CMEIAS computer-assisted microscopy at single-cell resolution. Diversity 5:426–460
11. Zahid W, Ganczarczyk J (1994) A technique for a characterization of RBC biofilm surface. Water Res 28:2229–2231
12. Hermanowicz S, Schindler U, Wilderer P (1995) Fractal structure of biofilms: new tools for investigation of morphology. Water Sci Technol 32:99–105
13. Yang X, Beyenal H, Harkin G, Lewandowski Z (2000) Quantifying biofilm structure using image analysis. J Microbiol Methods 39:109–119
14. Rojas D, Rueda L, Urrutia H, Carcamo G, Ngom A (2011) Biofilm image analysis: automatic segmentation methods and applications. In: Dua S, Acharya RU (eds) Data mining in biomedical imaging, signaling, and systems. CRC Press Taylor & Francis Group, Boca Raton, pp 319–349
15. Tolle CR, McJunkin TR, Stoner DL (2003) MAPPER: a software program for quantitative biofilm characterization. Technical Report, Idaho National Engineering and Environmental Laboratory. http://www.inl.gov/physics/d/asmhandout.pdf Accessed 6 May 2014
16. Ferreira T, Rasband W (2010) ImageJ User Guide. http://rsbweb.nih.gov/ij/docs/user-guide.pdf Accessed 6 May 2014
17. Sasaki H, Shibata S, Hatanaka T (1994) An evaluation method of ecotypes of Japanese lawn grass (*Zoysia japonica* STEUD.) for three different ecological functions. Bull Natl Grassl Res Inst 49: 17–24 (In Japanese with English summary, see<cse.naro.affrc.go.jp/sasaki/fractal/fractal-e.html>

18. 1McGarigal K Fragstats (2014) metrics http://www.umass.edu/landeco/research/fragstats/documents/Metrics/Shape%20Metrics/FRAGSTATS%20Metrics.htm (2014) Accessed 6 May 2014
19. Vuidel G (2014) Fractalyse fractal analysis software. http://www.fractalyse.org/en-home.html Accessed 6 May 2014
20. Cornforth D, Jelinek H, Peichl L (2002) Fractop: a tool for automated biological image classification. Presented at the 6th Australasia-Japan Joint Workshop, Australian National University, Canberra, Australia, 30-November–1 December 2002. 8 pp
21. Kenkel N, Walker D (1993) Fractals and ecology. Abstracia Bot 17: 53–70
22. Ji Z (2000) Quantitative analysis of biofilm images using fractal dimensions. Thesis, University of Memphis
23. Narasimhan G (2004) BIP: biofilm image processing. http://users.cis.fiu.edu/~giri/BIP Accessed 6 May 2014
24. Roberts A, Withers P (2012) StatistiXL ver. 1.10; Broadway-Nedlands: Kalamunda, Australia. http://www.statistixl.com/ Accessed 6 May 2014
25. Weisstein EW (2014) Fractal dimension. From MathWorld–A Wolfram Web Resource. http://mathworld.wolfram.com/FractalDimension.html Accessed 6 May 2014
26. Weisstein EW (2014) Capacity dimension. From MathWorld–A Wolfram Web Resource. http://mathworld.wolfram.com/CapacityDimension.html Accessed 6 May 2014
27. Allen M, Brown GJ, Miles NJ (1995) Measurement of boundary fractal dimensions : review of current techniques. Powder Technol 84:1–14
28. Bourke P (2003) FDC: fractal dimension calculator. http://paulbourke.net/fractals/fracdim/ Accessed 6 May 2014
29. Weisstein EW (2014) Least squares fitting. From MathWorld–A Wolfram Web Resource. http://mathworld.wolfram.com/LeastSquaresFitting.html Accessed 6 May 2014
30. Flook AG (1978) The use of dilation logic on the quantimet to achieve fractal dimension characterization of texture and structured profiles. Powder Technol 21:295–298
31. Iannaccone PM, Khokha M (1996) Fractal geometry in biological systems: an analytical approach. CRC Press, Boca Raton
32. McLachlan CS, Jelinek HF, Kummerfeld SK, Rummery N, McLachlan PD, Jusuf P, Driussi C, Yin J (2000) A method to determine the fractal dimension of the cross-sectional jaggedness of the infarct scar edge. Redox Rep 5:119–121
33. Milosevic NT, Ristanovic D, Stankovic JB (2005) Fractal analysis of the laminar organization of spinal cord neurons. J Neurosci Methods 146:198–204
34. Schwarz HB, Exner HE (1980) The implementation of the concept of fractal dimension on a semi-automatic image analyzer. Powder Technol 27:207–213
35. deBoer DH, Stone M, Lvesque LM (2000) Fractal dimensions of individual flocs and floc populations in streams. Hydrol Process 14: 653–667
36. Dellino P, Liotino G (2002) The fractal and multifractal dimension of volcanic ash particles contour: a test study on the utility and volcanological relevance. J Volcanol Geoth Res 113:1–18
37. Dazzo FB (2012) CMEIAS-aided microscopy of the spatial ecology of individual bacterial interactions involving cell-to-cell communication within biofilms. Sensors 12:7047–7062
38. Dazzo FB, Yanni YG (2013) CMEIAS: an improved computing technology for quantitative image analysis of root colonization by rhizobacteria *in situ* at single-cell resolution. In: DeBruijn F (ed) Molecular microbial ecology of the rhizosphere, vol 2, Chapter 69. J Wiley & Sons, New York, pp 733–742